THE ASTROPHYSICAL JOURNAL, 307:852–865, 1986 August 15

CHEMICAL MODELS OF THE DEEP ATMOSPHERE OF URANUS

BRUCE FEGLEY, JR., AND RONALD G. PRINN
Department of Earth, Atmospheric, and Planetary Sciences, Massachusetts Institute of Technology
Received 1986 January 10; accepted 1986 January 30

ABSTRACT

Results are presented for the first comprehensive chemical models of the deep atmosphere of Uranus. Bulk compositional models which are compatible with accepted chemical models of the solar nebula indicate that the atmosphere of Uranus may be enriched 100–1000 times in ice- and rock-forming elements relative to solar abundances. These models imply (1) the deep atmosphere is a H_2O–rich supercritical fluid and that water cloud condensation occurs at (or near) the pure H_2O critical point of 647 K; (2) several gases including NH_3, CH_4, and H_2 may be depleted above the water clouds by solution in the clouds; and (3) formation of Uranus from large reservoirs of disequilibrium C and N (e.g., carbonaceous chondrite-like organic matter, CO, CO_2, N_2 ices and clathrates) as first suggested by Lewis and Prinn, may (measurably) deplete H_2 by reactions to form CH_4 and NH_3. A plausible model enriched 500 times relative to solar abundances is described in detail. Thermochemical equilibrium calculations predict that N_2 is the most abundant nonequilibrium trace gas which can be mixed upward from Uranus's deep atmosphere. Other potential chemical probes of the deep atmosphere include PH_3, GeH_4, CO, CO_2, HCN, C_2H_6, CH_3OH, CH_3NH_2, CH_3SH, H_2Se, HCl, and HF. The effects of nonideal gas behavior and of assumed vertical mixing rates on the abundances of several of these species (N_2, PH_3, GeH_4, CO, CO_2, and HCN) are studied quantitatively. A complete treatment of nonideal gas effects including gas fugacity coefficients as functions of temperature and pressure and deviations from the ideal gas law shows that the abundances of N_2, CO, CO_2, and HCN are decreased by nonideal gas effects, while the abundances of PH_3 and GeH_4 are increased. Vertical eddy diffusion coefficients of 10^7–10^8 $cm^2\ s^{-1}$ yield a N_2 mixing ratio of $\approx$130 parts per million by volume (ppmv). This prediction takes nonideal gas behavior into account and is compatible with the (estimated) internal heat fluxes of 10–100 ergs $cm^{-2}\ s^{-1}$ due to radioactive heating (Danielson) or escaping primordial heat (Hubbard). Larger N_2 mixing ratios resulting from vertical mixing are inconsistent with the fugacity coefficients for H_2, N_2, and NH_3, with plausible vertical eddy diffusion coefficients, and with all plausible compositional models.

Subject headings: planets: abundances — planets: atmospheres — planets: Uranus

I. INTRODUCTION

The atmosphere of Uranus is fundamentally different from the atmospheres of Jupiter and Saturn. The average density of $\sim$1.3 g cm^{-3} and interior structure models require that Uranus is strongly enriched in heavy elements ($Z \geq 3$) relative to solar composition (Hubbard 1984; Hubbard and MacFarlane 1980; Prinn 1973; Reynolds and Summers 1965; Stevenson 1982*a*, *b*). Spectroscopic observations of CH_4 in the visible and near-IR regions imply CH_4/H_2 mixing ratios of 1%–10% (Baines 1983; Bergstralh and Baines 1984; Wallace 1980). Thermal radiance observations imply approximate equilibrium with absorbed sunlight and the absence of a significant internal heat source (Fazio *et al.* 1976; Loewenstein *et al.* 1977; Moseley, Conrath, and Silverberg 1985). These observations also imply that the deep atmosphere is both colder and denser (greater pressure at a given temperature) than the atmospheres of Jupiter and Saturn. Microwave spectra indicate an apparent depletion of NH_3 in the 150–200 K region of the atmosphere by 100–200 times relative to the solar NH_3/H_2 mixing ratio (de Pater and Massie 1985; Gulkis, Janssen, and Olsen 1978; Gulkis *et al.* 1983; Klein and Turegano 1978). Taken together, these observations show that existing models of the deep atmospheres of Jupiter and Saturn cannot be applied to Uranus. Instead it is essential to develop new models of the chemistry of the deep atmosphere of Uranus which can be used to interpret Earth-based, Earth-orbital, and *Voyager 2* spectroscopic data; to guide future observations; and ultimately to plan experiments on an entry probe mission.

In this paper we present results of the first set of comprehensive thermochemical equilibrium and where relevant nonequilibrium calculations on the chemistry of the deep atmosphere of Uranus. The calculations cover several important areas: (*a*) ideal gas thermochemical equilibrium calculations for several hundred gases of the most abundant and volatile elements, (*b*) real gas thermodynamic corrections, (*c*) condensation of cloud-forming materials, (*d*) effects of cloud formation on the chemistry, structure, and dynamics of the deep atmosphere, and (*e*) thermochemical kinetics of the important destruction reactions for potential chemical probes (e.g., N_2, PH_3, GeH_4, CO, CO_2, HCN) of the deep atmosphere. Our results demonstrate that contrary to popular belief, it is essential to consider fugacity coefficients as well as incompressibility effects to calculate properly the thermodynamic behavior of real gases in the deep atmosphere of Uranus. Finally we also consider the influence of widely varying elemental compositions and vertical mixing rates in our models.

II. GENERIC BULK COMPOSITION AND ATMOSPHERIC MODELS

A consideration of the chemistry of the major elements in the solar nebula, scenarios for the formation of Uranus, interior structure models, and spectroscopic data on the CH_4/H_2 mixing ratio constrains acceptable planetary bulk composi-

tions and provides guidelines for constructing atmospheric composition models.

The two general scenarios for the origin of Uranus, Jupiter, Saturn, and Neptune involve either direct collapse of nebular gas and grains (e.g., see Cameron 1978*a*, *b*) or collapse of nebular gas and grains onto a preformed solid core (Perri and Cameron 1974; Mizuno 1980). Because the directly collapsed planet can subsequently capture solid material, both scenarios predict planets which potentially are enriched to varying degrees in ice- and rock-forming elements over their solar composition values. We can therefore consider the two models equivalent for this work.

The retention of different volatiles (e.g., CH_4, CO, NH_3, N_2) by the solids which accreted to form Uranus depended on the (P, T) profile and chemistry of the solar nebula when Uranus formed and the rates at which the accretion of grains and the cooling of the nebula proceeded relative to gas-condensate reaction rates. Although these parameters are not well constrained, eight classes of generic models describe the effects of different extreme assumptions about these parameters on volatile retention by Uranus (see Lewis 1972*a*, *b*; Barshay and Lewis 1976; Fegley and Lewis 1980; Lewis and Prinn 1980; Prinn 1982; Prinn and Fegley 1981; Prinn and Lewis 1973 for complete descriptions of this approach). Table 1 outlines the eight classes of generic models and gives the relative mass fractions for all condensates.

The condensate mass fractions in Table 1 were calculated using Cameron's (1982) solar abundances. For these calculations "rock" was taken as $SiO_2 + MgO + CaO + Al_2O_3 + TiO_2 + Fe + FeS$, the H_2O ice abundance was corrected for the amount of oxygen in "rock," hydrates, and clathrates, the solid solution of N_2 in CO clathrate was considered (Lunine and Stevenson 1985), and all sulfur was put into NH_4SH (instead of FeS in "rock") for all fast (inhomogeneous) accretion models.

TABLE 1

GENERIC MODELS FOR COMPOSITION OF CONDENSATES INCORPORATED INTO URANUS

	I. SLOW (HOMOGENEOUS) ACCRETION[a]
A.	Low temperatures ($5\ K < T \leq 20\ K$)[b]
1.	*Complete equilibrium:* "Rock"[c] (0.26) + $NH_3 \cdot H_2O$ (0.12) + $CH_4 \cdot 6H_2O$ (0.40) + CH_4 ice (0.21) + Ar ice (0.006)
2.	*Kinetic inhibition:* "Rock" (0.30) + $N_2 \cdot 6H_2O$ (0.08) + $CO \cdot 6H_2O$ (0.08) + N_2 ice (0.04) + CO ice (0.50) + Ar ice (0.007) + CO_2 ice (0.008) + NH_3 ice (0.0007)
B.	High temperatures ($T \approx 50\ K$)
3.	*Complete equilibrium:* "Rock" (0.34) + $NH_3 \cdot H_2O$ (0.15) + $CH_4 \cdot 6H_2O$ (0.51)
4.	*Kinetic inhibition:* "Rock" (0.64) + $N_2 \cdot 6H_2O$ (0.02) + $CO \cdot 6H_2O$ (0.32) + CO_2 ice (0.02) + NH_3 ice (0.001)
	II. FAST (INHOMOGENEOUS) ACCRETION[d]
A.	Low temperatures ($5\ K < T \leq 20\ K$)
5.	*Complete equilibrium:* "Rock" (0.24) + H_2O ice (0.41) + NH_3 ice (0.04) + NH_4SH ice (0.04) + CH_4 ice (0.26) + Ar ice (0.006)
6.	*Kinetic inhibition:* "Rock" (0.27) + H_2O ice (0.12) + N_2 ice (0.05) + CO ice (0.51) + Ar ice (0.007) + CO_2 ice (0.008) + NH_4SH ice (0.002) + H_2S ice (0.03)
B.	High temperatures ($T \approx 50\ K$)
7.	*Complete equilibrium:* "Rock" (0.33) + H_2O ice (0.56) + NH_3 ice (0.06) + NH_4SH ice (0.05)
8.	*Kinetic inhibition:* "Rock" (0.63) + H_2O ice (0.29) + CO_2 ice (0.02) + NH_4SH ice (0.004) + H_2S ice (0.06)

[a] Accretion of grains and cooling of the nebula are assumed to be slow relative to gas-condensate reaction rates, so that complete gas-solid equilibrium is attained (Lewis 1972*a*).

[b] Complete descriptions of the low-temperature condensation sequence in the solar nebula are given elsewhere (Lewis 1972*a*; Lewis and Prinn 1980; Prinn and Fegley 1981).

[c] Rock = $SiO_2 + MgO + Al_2O_3 + TiO_2 + CaO + FeS + Fe$. All S as NH_4SH(s) and not FeS in fast accretion models.

[d] Accretion and cooling are assumed to be fast relative to gas-condensate reaction rates so that a condensate once formed becomes removed from further reactions (Lewis 1972*a*).

An important implication of the kinetic inhibition models (Nos. 2, 4, 6, 8) in Table 1 is that if Uranus formed from large reservoirs of disequilibrium C and N (e.g., carbonaceous chondrite-like organic matter; CO, CO_2, N_2 ices and clathrates) as first suggested by Lewis and Prinn (1980), then H_2 may be (measurably) depleted by reactions to form CH_4 and NH_3. This depletion will increase the He/H_2 mixing ratio over the solar value of 0.135 (Cameron 1982). Model 2 in Tables 1 and 2 is an extreme example of this effect. H_2 depletion by reactions with disequilibrium C and N reservoirs such as the organic matter in carbonaceous material will be less pronounced at equivalent C and N enrichment levels over solar abundances.

The four low-temperature accretion models (Nos. 1, 2, 5, 6) in Table 1 can be represented by models 1 and 2 because there is no difference between models 1 and 5, or 2 and 6 for our purposes. Furthermore, Table 1 shows that either carbon-free (No. 7) or carbon-poor (No. 8) assemblages result if fast (inhomogeneous) accretion at ~ 50 K is assumed. Model 8 exemplifies the latter two low-carbon cases. We note that the chemistry and mineralogy of chondritic meteorites are better explained by the slow (homogeneous) accretion sequence (e.g., see Larimer 1967; Larimer and Anders 1967, 1970). Further discussion here focuses on the exemplary class 1, 2, 3, 4, and 8 models.

During the formation of Uranus, enrichment of the ice- and rock-forming elements relative to their solar composition abundances may occur to varying degrees depending on the relative proportions of nebular gas and grains accreted by Uranus. Representative gas/solid and ice/rock ratios and element/H_2 mixing ratios, which were calculated as a function of assumed grain enrichment factors using Table 1 and Cameron's (1982) solar abundances, are displayed in Table 2. The gas/solid ratio in Uranus deduced from the bulk density and interior structure models ranges from 11:89 to 25:75 by mass (Hubbard 1984; Hubbard and MacFarlane 1980; Stevenson 1982*b*). Table 2 illustrates that enrichment factors between 100 to 1000 times greater than solar are required to give gas/solid ratios consistent with the values above. Models with ice/rock ratios (I/R) of 2.0–2.8 require enrichment factors between 100 to 500 times, while models with smaller I/R values of ~ 0.6 require larger enrichment factors between 500 to 1000 times to be consistent with gas/solid mass fractions of 11:89 to 25:75. However, *all* classes of models considered indicate that it is necessary to study Uranus models with enrichment factors greater than 100 times solar for the ice- and rock-forming elements.

The preferred models in Table 2 are those which are consistent with the independently estimated gas/solid ratio, the ice/rock ratio inferred from the J_2 and ϵ values ($I/R > 1$; see Hubbard 1984; Podolak and Reynolds 1984), and CH_4/H_2 mixing ratios from 1% to 10% (Baines 1983; Bergstralh and Baines 1984; Wallace 1980). The inferred NH_3/H_2 mixing ratio (de Pater and Massie 1985; Fink and Larson 1979; Gulkis, Janssen, and Olsen 1978; Gulkis *et al.* 1983; Klein and Turegano 1978) is not used as a constraint because the NH_3/H_2

TABLE 2

URANUS BULK COMPOSITION AND ATMOSPHERE MODELS

Model	Enrichment Factor[a]	Mass Percentages[b]				Mixing Ratios			
		Gas	Ice	Rock	I/R	C/H_2	N/H_2	He/H_2	μ[c]
1.....	10×	84	12	4	2.8	8.3×10^{-3}	1.7×10^{-3}	0.135	2.54
	50×[d]	50	37	13	2.8	4.2×10^{-2}	8.7×10^{-3}	0.135	3.57
	100×[d]	34	49	17	2.8	8.3×10^{-2}	1.7×10^{-2}	0.135	4.68
	500×	9	67	24	2.8	4.2×10^{-1}	8.7×10^{-2}	0.135	9.77
2.....	10×	83	12	4	2.4	8.6×10^{-3}	1.8×10^{-3}	0.139	2.56
	50×[d]	48	38	14	2.4	4.8×10^{-2}	1.0×10^{-2}	0.157	3.80
	100×[d]	30	52	18	2.4	1.2×10^{-1}	2.4×10^{-2}	0.187	5.43
	500×[e]	2	72	26	2.4	∞	∞	∞	17.29
3.....	10×	87	9	4	2.0	2.3×10^{-3}	1.7×10^{-3}	0.135	2.47
	50×	56	29	15	2.0	8.8×10^{-3}	8.7×10^{-3}	0.135	3.26
	100×[d]	39	40	20	2.0	1.7×10^{-2}	1.7×10^{-2}	0.135	4.13
	500×[d,f]	11	59	30	2.0	8.2×10^{-2}	8.7×10^{-2}	0.135	8.60
4[g].....	10×	92	3	5	0.6	1.3×10^{-3}	2.6×10^{-4}	0.136	2.33
	50×	71	10	18	0.6	3.7×10^{-3}	6.0×10^{-4}	0.137	2.62
	100×	55	16	29	0.6	6.6×10^{-3}	1.0×10^{-3}	0.138	2.97
	500×[d,f]	20	29	51	0.6	3.2×10^{-2}	5.1×10^{-3}	0.150	5.43
	1000×[d,f]	11	32	57	0.6	6.7×10^{-2}	1.1×10^{-2}	0.168	7.95
8[g].....	10×	93	3	5	0.6	9.1×10^{-4}	1.0×10^{-4}	0.135	2.32
	50×	72	10	17	0.6	1.2×10^{-3}	2.6×10^{-4}	0.135	2.54
	100×	57	16	27	0.6	1.7×10^{-3}	3.5×10^{-4}	0.135	2.81
	500×[f]	21	30	50	0.6	4.7×10^{-3}	1.0×10^{-3}	0.138	4.74
	1000×[f]	12	33	56	0.6	8.6×10^{-3}	1.9×10^{-3}	0.140	6.63
	10000×	2	36	63	0.6	1.1×10^{-1}	2.6×10^{-2}	0.194	16.43

[a] Enrichments calculated relative to Cameron 1982 solar abundances.

[b] Percentages may not total 100% because of round-off errors.

[c] Mean molecular weight of the atmosphere before condensation of aqueous solution clouds. $\mu = \Sigma x_i \mu_i$ for H_2, He, H_2O, CH_4, NH_3, H_2S, Ar, and Ne.

[d] Model C/H_2 mixing ratio agrees with CH_4/H_2 mixing ratio of 1%–10% (Wallace 1980; Baines 1983; Bergstralh and Baines 1984).

[e] All H_2 consumed by reactions forming CH_4 and NH_3 from CO, CO_2 and N_2 ($CO + 3H_2 = CH_4 + H_2O$, $CO_2 + 4H_2 = CH_4 + 2H_2O$ and $3H_2 + 2N_2 = 2NH_3$).

[f] Calculated mass percentages of gas, ice, and rock agree with estimated gas/(ice + rock) ratios of 11:89 (Hubbard and MacFarlane 1980), 25:75 to 11:89 (Stevenson 1982*b*), and 19:81 (Hubbard 1984).

[g] Disagrees with inferences based on J_2 and ϵ which favor $I/R > 1$ (Hubbard 1984, and references therein).

mixing ratios calculated by considering NH_3 solution in water clouds and NH_4SH condensation (Atreya and Romani 1985; Fegley and Prinn 1985*a*) are compatible with the NH_3 depletions inferred from the microwave and infrared data.

The only model which satisfies all three constraints is the class 3 model enriched 500 times. Although it may appear too CH_4–rich, substantial amounts of CH_4 can dissolve in the water clouds and thus reduce the CH_4/H_2 mixing ratio in the observable atmosphere (see § IV*a*). Table 2 also shows that the class 4 models which are enriched 500 and 1000 times relative to solar composition are also consistent with the gas/solid ratio and CH_4/H_2 mixing ratio but not with the inferred I/R value. However, the I/R value for Uranus is not well defined and if it is greater than 1, may have been increased from the lower values predicted by the class 4 models by several plausible processes such as chemical reprocessing of CO and N_2 in a Uranus subnebula (e.g., see Prinn and Fegley 1981) or by the subsequent accretion of ice-rich planetesimals. In the absence of firm constraints on the Uranian ice/rock ratio we will discuss the implications of all three models for the chemistry of the deep atmosphere of Uranus.

Finally, our generic models cover most (but not all) possible bulk compositions and atmospheric compositions for Uranus. We assume that all C, N, and O are in the atmosphere; however, other (less well constrained) scenarios such as partitioning of O, C, and N between the atmosphere and interior can also be discussed using the range of models we consider.

III. CONSTRUCTION OF URANUS ATMOSPHERE MODELS

Orton, Tokunaga, and Caldwell (1983), Orton and Appleby (1984), and Moseley, Conrath, and Silverberg (1985) summarize thermal radiance observations which indicate temperature minima of 53–55 K near 200 mbar, a radiative-convective boundary at 400–500 mbar, and temperatures around 74 K at 1 bar. However, the assumption of an adiabatic gradient in the deep atmosphere is debatable because of the apparent lack of a significant internal heat source on Uranus (Orton and Appleby 1984, and references therein). Nevertheless, Hubbard (1978) estimated that the remaining primordial heat escaping from Uranus is ~ 100 ergs cm^{-2} s^{-1}, which is apparently sufficient to maintain convection throughout the atmosphere (Hunten 1984; Wallace 1980). Also, thermal emission from the deep Uranus atmosphere with temperature increasing with depth is the preferred model to explain the observed microwave spectra (Gulkis and de Pater 1984). For these reasons interior structure models (e.g., Hubbard 1984, and references therein) assume an adiabatic gradient.

a) *Ideal Gas Models*

We assume specifically here that the temperature gradient in the atmosphere beneath the radiative-convective boundary is adiabatic and take temperature $T = 74$ K at total pressure $P = 1$ bar. Dry adiabatic lapse rates in the deep atmosphere are then calculated stepwise using the method described by Fegley and Prinn (1985*b*) with the globally averaged acceleration of gravity taken as 900 cm s^{-2}. Wet adiabatic lapse rates in the deep atmosphere due to the condensation of aqueous solution clouds were calculated from the expression (Hess 1959, pp. 39–113; Lasker 1963):

$$(\partial \ln T/\partial \ln P)_s = [1 + (1 + \alpha)(P_w/P_d)] \times [(C_p/R)_d + X_w(C_p/R)_w + X_A(C_p/R)_A + (P_w/P_d)(\alpha + \alpha^2)]^{-1}, \quad (1)$$

where the subscripts w, d, and A refer, respectively, to water, dry atmospheric gas, and ammonia; X_i is the (variable) mixing ratio of i, P_w is the saturated vapor pressure for water from Keenan *et al.* (1969), α is $\Delta H_{vap}/RT$, R is the gas constant, and ΔH_{vap} is the temperature-dependent heat of vaporization along the saturation curve (Keenan *et al.* 1969). The change in P_w due to the decreased water vapor pressure above concentrated aqueous NH_3 solutions was considered using the aqueous NH_3 solution vapor pressure data of Scatchard *et al.* (1947). Changes in ΔH_{vap} with solution composition were not considered because they are appreciable only at low temperatures where $(P_w/P_d)(1 + \alpha) \ll 1$ and $(P_w/P_d)(\alpha + \alpha^2) \ll (C_p/R)_d$ and are thus unimportant for defining the lapse rate. The heat capacity at constant pressure (C_p) data for H_2, He, Ne, Ar, H_2O, CH_4, NH_3, and H_2S, as functions of temperature which were used in the calculations, were taken from the JANAF tables and supplements (Stull and Prophet 1971; Chase *et al.* 1971–1985).

b) *Real Gas Models*

The real H_2(g) adiabat was calculated from the equation for an incompressible fluid adiabatic gradient (Rowlinson and Swinton 1982)

$$(\partial T/\partial P)_s = TV\alpha_p/C_p, \quad (2)$$

where α_p is the isobaric coefficient of thermal expansion and V is the molar volume. The equation of state for fluid H_2 (Mills *et al.* 1977), α_p values calculated from their data, and C_p data from Mills *et al.* (1977) and the JANAF tables were used in the calculations. The Mills *et al.* (1977) equation of state and its derivatives remain regular when extrapolated to very high (P, T) values. Their equation of state also gives reasonable agreement with experimental data and other equations of state well beyond the range of (P, T) values which were studied experimentally (see Mills *et al.* 1977 for details).

c) *Computed Profiles*

Figure 1 illustrates resultant Uranus model atmospheres as a function of temperature and pressure. Also shown are adiabats for the solar nebula model of Lewis and Prinn (1980) and for a present-day Jupiter model. The Jovian ideal gas adiabat is calculated taking $T = 165$ K at $P = 1$ bar (Lindal *et al.* 1981) and Cameron's (1982) solar abundances. The Uranus adiabats are calculated for ideal H_2(g), real H_2(g), and for our class 3 model enriched 500 times with ideal H_2(g). All the other Uranus adiabats considered fall within the limits defined by the three Uranus adiabats in Figure 1.

Figure 1 shows that the real and ideal H_2(g) adiabats are fairly close together except at the highest pressures and temperatures. At 1000 K, which is a representative quench temperature for nonequilibrium trace gases in the Uranian deep atmosphere (Fegley and Prinn 1985*a*), the pressures on the real and ideal H_2(g) adiabats are $10^{3.5}$ and $10^{3.7}$ bars, respectively. By 2500 K, well above the plausible quench temperatures for any nonequilibrium gases, the ideal H_2(g) adiabat is still only a factor of 2 higher pressure than the real gas adiabat. Also, at the hypothesized gas/ice boundary ($T \approx 2500$ K) calculated by Hubbard and MacFarlane (1980), our real H_2(g) adiabat gives $P \approx 100$ kbar and $\rho \approx 0.2$ g cm^{-3} versus $P \approx 220$ kbar and $\rho \approx 0.4$ g cm^{-3} in their interior model.

IV. RESULTS OF THERMOCHEMICAL EQUILIBRIUM CALCULATIONS

a) *Ideal Gas Equilibria*

Detailed calculations of thermochemical equilibria were done for the elements H, O, C, N, Mg, Si, Fe, S, P, Cl, F, Ge, and Se, which were chosen on the basis of their solar abundance (Cameron 1982) and volatility. Thermodynamic data for these calculations were taken from standard sources (Chase *et al.* 1971–1985; Glushko *et al.* 1978–1982; Kelley 1937, 1960; Kelley and King 1961; Stull and Prophet 1971; Stull, Westrum, and Sinke 1969; Wagman *et al.* 1968). We scaled thermodynamic calculations for many other elements, which are less interesting because of lower abundances or lower volatilities or both, from Jupiter's atmosphere (Lewis 1969*a*; Barshay and Lewis 1978; Fegley and Lewis 1979) to Uranus's atmosphere. This procedure is illustrated for Saturn by Prinn *et al.* (1984) and is applicable for Uranus by using appropriate T, P, and composition values. Our calculations therefore give upper limits to the abundances of ~700 compounds of 44 elements (see Lewis 1969*a*; Barshay and Lewis 1978; Fegley and Lewis 1979 for a complete listing of all compounds and elements considered).

We calculated the solubilities of H_2, He, CH_4, NH_3, N_2, H_2S, Ne, and Ar in the aqueous solution clouds as a function of temperature and pressure. Temperature-dependent Henry's law constants for H_2, N_2, He, Ne, Ar (Clever and Han 1980), NH_3 and H_2S (Roberts and Tremaine 1985), and CH_4 solubility data in water as a function of T and P (Culberson and McKetta 1951; DeLoos, Wijen, and Diepen 1980; Larsen and Prausnitz 1984; Price 1979; Sultanov, Skripka, and Namiot 1971, 1972*a*, *b*) were used. Gas solubilities (except CH_4) in the aqueous solution clouds were estimated using the Krichevsky-Kasarnovsky equation (Reid, Prausnitz, and Sherwood 1977):

$$\ln (p/x)_g = \ln (XP/x)_g = \ln H_g + [\bar{V}_g^{\infty}(P - P_w)/RT], \quad (3)$$

where subscript g denotes the gaseous solute; p is the partial pressure of the gaseous solute; x is the liquid-phase mole fraction; X is the vapor-phase mixing ratio; H_g is the Henry's law constant with units of bars, and $\bar{V}^{\infty}$ is the partial molar volume at infinite dilution in the liquid phase. Except for Ar, the $\bar{V}^{\infty}$ values were taken from the same sources as the Henry's law constants; since no Ar value was available, we took its $\bar{V}^{\infty}$ value to be equal to that for Ne. The solubility of CH_4 in the aqueous solution clouds was calculated from the data of DeLoos, Wijen, and Diepen (1980), Larsen and Prausnitz (1984), and Sultanov, Skripka, and Namiot (1971, 1972*a*, *b*). These data sets are the most reliable for CH_4 at (P, T) conditions near the pure H_2O critical point.

The solubilities of gases other than those discussed above in

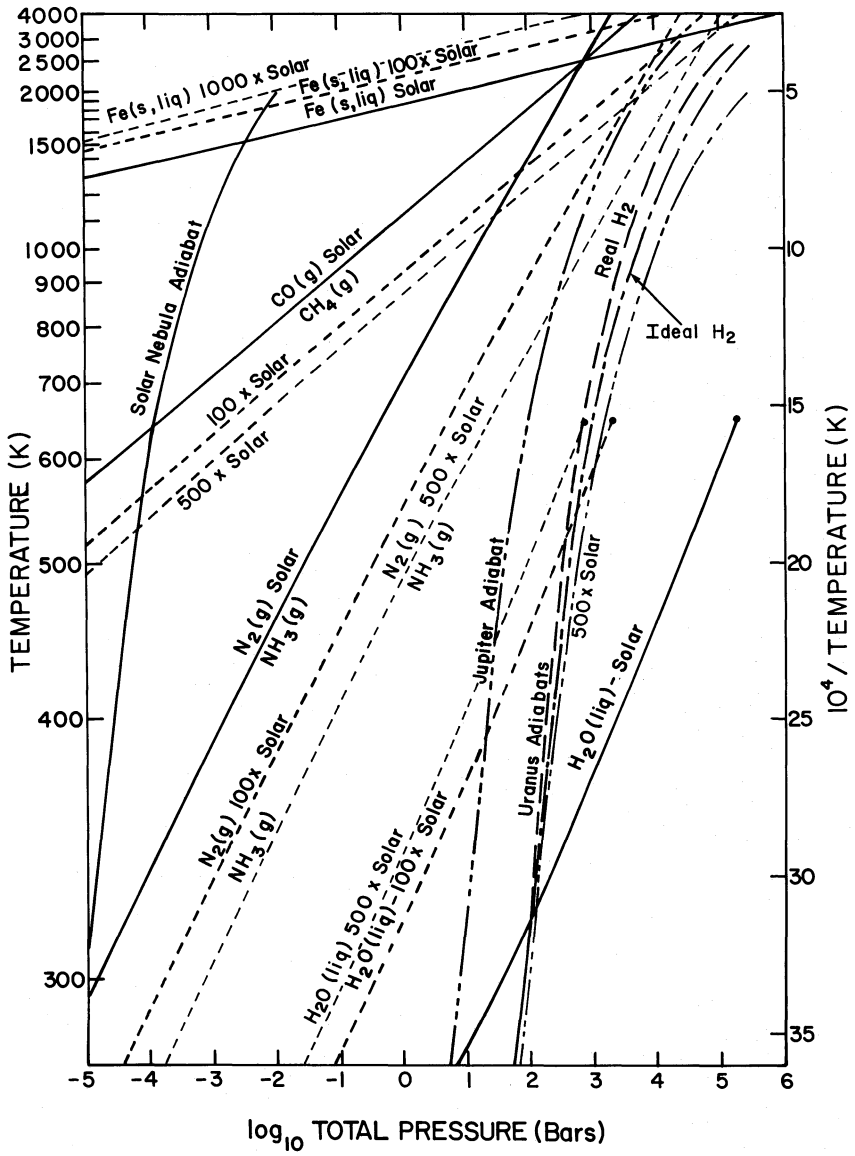

FIG. 1.—Some features of the equilibrium chemistry of solar composition gas and of Uranus model atmospheres as functions of temperature and pressure. Adiabats for the solar nebula, the Jovian atmosphere, and the Uranian atmosphere are illustrated in relation to the stability fields of Fe(s, liquid) and liquid H_2O. Regions where CO or CH_4 and N_2 or NH_3 are the dominant carbon and nitrogen bearing gases, respectively, are also shown. Lines labeled CO–CH_4 and N_2–NH_3 denote boundaries where the abundances of the two gases are equal. Several curves corresponding to different elemental enrichments relative to solar composition abundances are shown as dotted lines. The three Uranus adiabats cover the range of (P, T) profiles we considered and are described in the text. Points at the end of the H_2O condensation curves mark the pure H_2O critical temperature of 647 K.

the aqueous solution clouds were estimated only approximately by assuming the 298 K value of the Henry's law constant as calculated from data in Wagman *et al.* (1968) applies at all temperatures. Linear extrapolation ($\log_{10} H_g$ vs. $1/T$) of these constants to higher temperatures is incorrect because gas solubilities generally decrease, go through a minimum, and then increase as temperature increases toward the solvent's critical temperature (Reid, Prausnitz, and Sherwood 1977; Hayduk and Laudie 1973; Clever and Han 1980). No intrasolute interactions (e.g., salting out effects or compound formation) were considered because the required data at high P and T are unavailable. For example, data on the NH_3–H_2S–H_2O system (van Krevelen, Heftijzer, and Huntjens 1949; Leyko 1964) at 293–333 K are not useful because they cannot be extrapolated outside this range.

The thermochemical equilibrium calculations were done by standard methods which are described by Barshay and Lewis (1978). The calculations, which simultaneously consider mass balance and chemical equilibrium constraints, were done at temperatures ranging from 300 to 3000 K along the different adiabatic profiles. Some condensation processes at lower temperatures were also considered. The effects of condensation and of gas solubility in the aqueous solution clouds upon gas-phase mixing ratios, on mass balance, and on the calculated lapse rates was also properly accounted for (e.g., see Lewis 1969*b*).

Figure 1 illustrates several general thermochemical equilibrium points. First, as we move along the solar nebula adiabat toward the proto-Sun or along the planetary adiabats deeper into the atmospheres of Jupiter and Uranus, then CO

and N_2 become increasingly more stable relative to CH_4 and NH_3, respectively. However, while CO and N_2 become the major carbon and nitrogen bearing gases at thermochemical equilibrium in the inner regions of the solar nebula, they remain minor constituents throughout the deep atmospheres of Jupiter, Saturn, and Uranus (Prinn and Barshay 1977; Barshay and Lewis 1978; Prinn and Olaguer 1981; Fegley and Prinn 1985*a*, *b*). Second, the liquid H_2O condensation curve in Figure 1 shifts to the upper left (lower P, higher T) as enrichment factors increase. Thus, H_2O clouds will form at higher temperatures (and greater depths) in the Uranus atmosphere as the H_2O abundance is increased until the pure H_2O critical temperature of 647 K is reached. This temperature is the upper temperature limit for condensation of aqueous solution clouds (Fegley and Prinn 1985*a*) because the critical temperatures of NH_3–H_2O solutions (Tsiklis, Linshits, and Goryunova 1965) and of CH_4–H_2O solutions ($X_{CH_4} \leq 0.3$; DeLoos, Wijen, and Diepen 1980) are lower than those of pure H_2O, while those for H_2–H_2O solutions are only slightly higher ($T_c \approx 656$ K, $X_{H_2} \approx 0.4$; Seward and Franck 1981). Presumably, the opposing effects of NH_3 and CH_4 and of H_2 on the critical temperature will tend to cancel out, but no experimental data are available. Last, the Fe(s, liquid) condensation curves in Figure 1 also shift to lower P, higher T as the Fe abundance is enriched over solar composition. Because the calculated Uranus adiabats do not cross the Fe condensation curves, the presence of Fe particles, which may catalyze the N_2–NH_3 and CO–CH_4 conversions (Prinn and Olaguer 1981; Fegley and Prinn 1985*b*), in the deep atmosphere is very unlikely.

The results of thermochemical equilibrium calculations along the ideal, 500 times solar adiabat are displayed in Figures 2–5. These results can be compared to those for a 100 times solar adiabat in Fegley and Prinn (1985*a*). The most abundant gas is H_2, but H_2O (and not He) is the second most abundant gas below the solution cloud base at $T > 647$ K. Also, NH_3 is slightly more abundant than CH_4 below the solution clouds because this model assumes (incomplete) CH_4 retention as a clathrate (see Table 1). However, CH_4 is more abundant than NH_3 in some other generic models (Nos. 1, 2, 4, 5, 6, 8 in Table 1).

The 500 times solar model has a supercritical H_2O-bearing fluid at $T > 647$ K. At $\sim$647 K a large fraction ($\sim$54%) of the H_2O condenses. The composition of the initial H_2O–rich condensate, which is given in Table 3, shows that CH_4, H_2, and NH_3 are the most important solutes and that each has a mole fraction of $\sim$0.1. Qualitatively similar predictions for the composition of the initial H_2O–rich fluid were made by Stevenson (1984).

The gas-phase mixing ratios of several gases in the Uranian upper atmosphere may be reduced because of gas solubility in the aqueous solution clouds. The exact reduction will depend on the atmospheric composition and (P, T) profile. However,

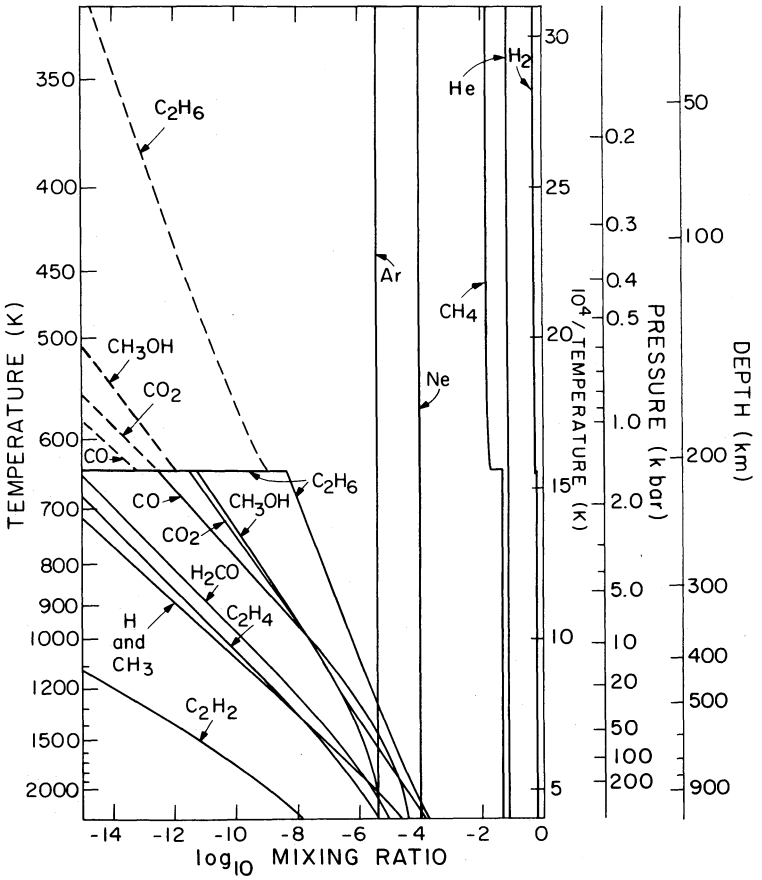

FIG. 2.—Equilibrium abundances of some carbon-containing gases along the 500 times enriched adiabat shown in Fig. 1. Volume mixing ratios are plotted as a function of inverse temperature. Discontinuities in the abundance curves at 647 K correspond to solution of gases in the aqueous solution clouds. Dotted lines show the abundances of several gases in the absence of any solubility in the water clouds. This is done where temperature-dependent Henry's law coefficients are unavailable. Vertical scales indicate temperature, pressure (dry lapse rate), and depth (below the 300 K level) along the model Uranus adiabat.

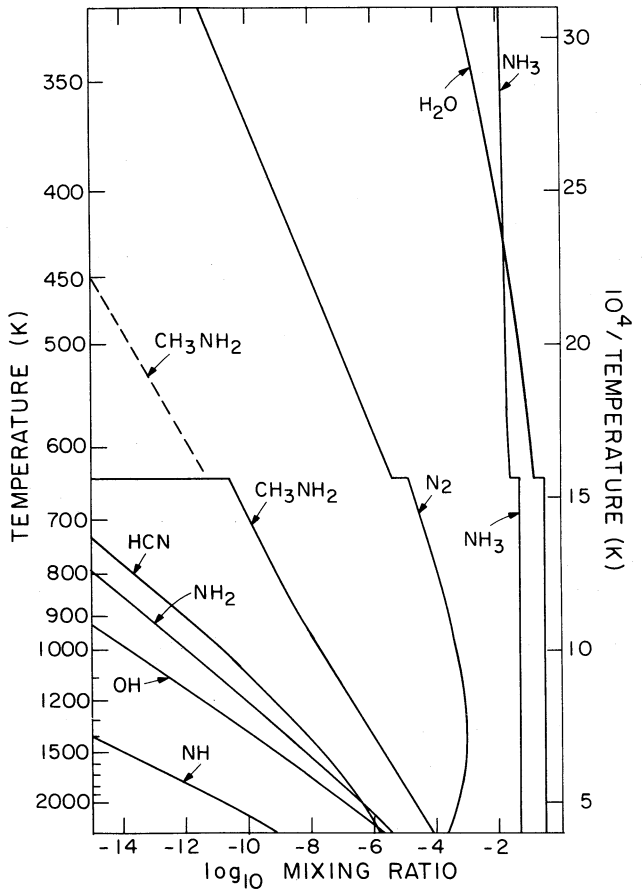

FIG. 3.—As in Fig. 2, but for oxygen- and nitrogen-containing gases. The abrupt formation of aqueous solution clouds at 647 K causes discontinuities in the abundance curves. See text for details.

for the 500 times solar model the H_2/He ratio in the atmosphere above the solution clouds is ~2% lower than its (solar) value beneath the clouds. Also, ~26% of available CH_4 and 71% of available NH_3 dissolve in the solution clouds. The NH_3 mixing ratio is further reduced by the condensation of NH_4HS(s) at ~320 K.

Several authors (Atreya 1983, 1984; Atreya and Romani 1985; Fegley and Prinn 1985*a*; Stevenson 1984) have stated that the depletion of NH_3 in the aqueous solution clouds will appreciably reduce the NH_3 mixing ratio in the Uranian upper atmosphere. The calculations for our different generic models confirm this prediction (e.g., for a 100 times solar model studied by Fegley and Prinn 1985*a*, the NH_3 mixing ratio varies from $\sim 10^{-9}$ at 200 K to $\sim 10^{-14}$ at 160 K). However, the solubility of other gases (e.g., H_2, CH_4, He) in the aqueous solution clouds is a general phenomenon and may cause depletions of several species (especially CH_4) in the visible Uranus atmosphere. Thus we caution that the CH_4/H_2 mixing ratio in the visible Uranus atmosphere may be appreciably lower than the CH_4/H_2 ratio in the deep atmosphere beneath the aqueous solution cloud base.

The condensation of the aqueous solution clouds also affects the abundances of trace gases in the deep atmosphere. Figures 2–5 show trace gas curves with discontinuities at the cloud base level which occur at 647 K. These are due to (1) the trace gas solubility in the solution clouds and (2) the reduction in thermochemical equilibrium abundances due indirectly to the

TABLE 3

COMPOSITION OF INITIAL H_2O-RICH FLUID (T = 647 K)[a]

Species	Liquid-Phase Mole Fraction
H_2O	0.72
CH_4	0.10
H_2	0.09
NH_3	0.09
He	6×10^{-3}
H_2S	4×10^{-3}
Ne	4×10^{-6}
H_2Se[b]	3×10^{-6}
Ar	2×10^{-7}
N_2	4×10^{-8}

[a] 500 times solar class 3 model.
[b] Estimated using Henry's law constant at 298 K (Wagman *et al.* 1968).

reduction in elemental fugacities. For example, N_2 is only sparingly soluble in the clouds ($X_{N_2} \approx 4 \times 10^{-8}$ in the aqueous solution), but its equilibrium abundance is also decreased by the reduction in the N_2 fugacity due to NH_3 solubility in the clouds. The solubilities of the trace gases C_2H_6, CH_3OH, CO_2,

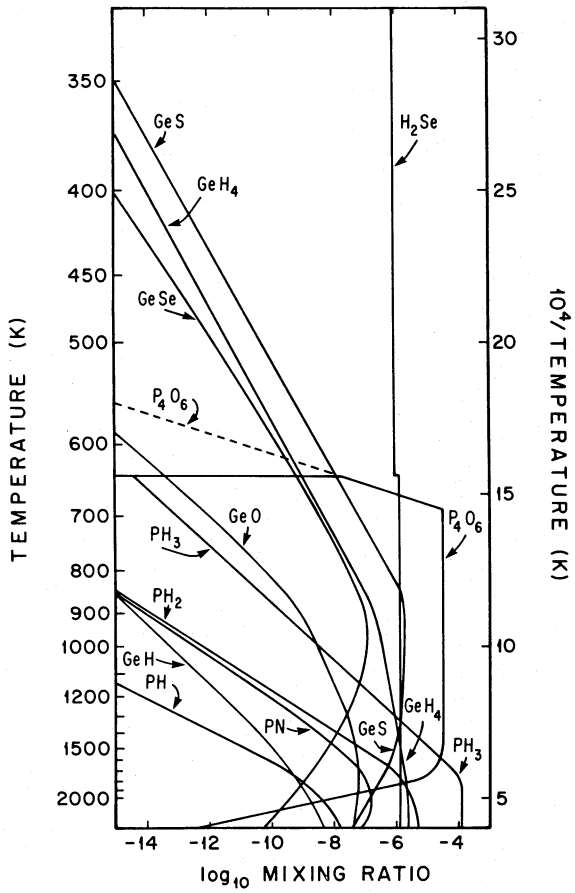

FIG. 4.—As in Fig. 2, but for phosphorus, germanium-, and selenium-containing gases. Ge(s) condenses at 888 K, and GeSe(s) condenses at 471 K. No Henry's law coefficients are available for any Ge-bearing gases, and solubility in the solution clouds cannot be calculated. $NH_4H_2PO_4$(s) condenses at 689 K and probably dissolves in the solution clouds at ~647 K. Dotted line shows the P_4O_6(s) abundance if solubility is not considered.

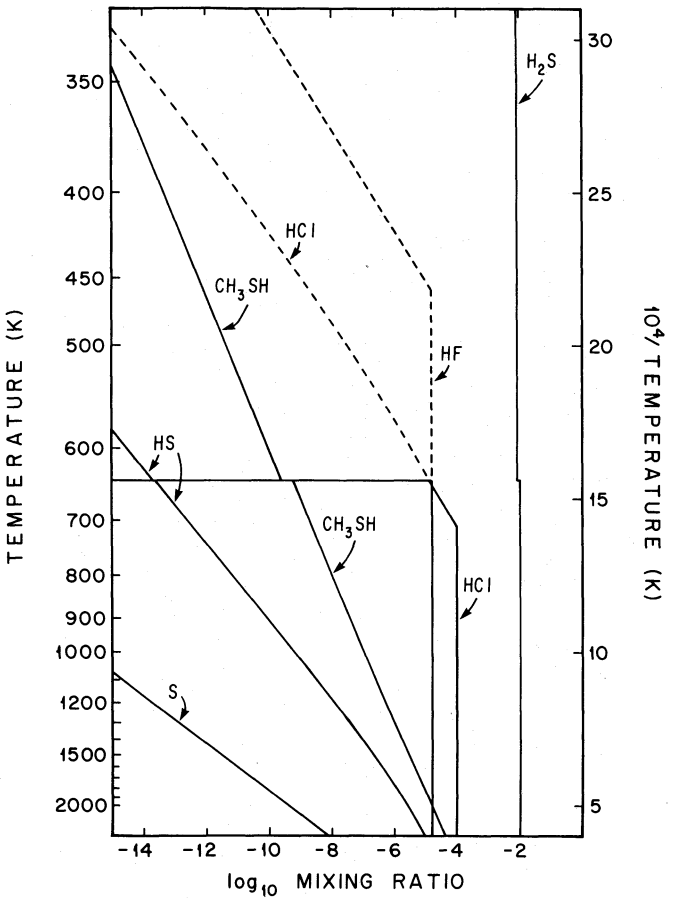

FIG. 5.—As in Fig. 2, but for sulfur-, chlorine-, and fluorine-containing gases. CH_3SH solubility is not considered because no Henry's law constant is available. Dotted lines show the HCl and HF abundances in the absence of any solubility in the aqueous clouds. In this case NH_4F(s) forms at 458 K.

CO, CH_3NH_2, HF, HCl were estimated only approximately by using Henry's law constants at 298 K for reasons discussed earlier. In these cases the absolute upper limits for the gas mixing ratios are the dotted lines (calculated neglecting any solubility in the aqueous clouds). No solubility estimates were made for GeH_4 and CH_3SH because no Henry's law constants were available in the NBS compilation (Wagman *et al.* 1968).

b) Real Gas Equilibria

The equilibrium constant expressions for the thermochemical equilibria between N_2–NH_3, CO–CH_4, CO_2–CH_4, HCN–NH_3, PH_3–P_4O_6, and GeH_4–GeS can be arranged to yield the relations

$$X_{N_2} = K_4 \phi^2_{NH_3}/(\phi_{N_2} \phi^3_{H_2})(X^2_{NH_3}/X^3_{H_2})(1/P^2) , \quad (4)$$

$$X_{CO} = K_5(\phi_{CH_4} \phi_{H_2O})/(\phi_{CO} \phi^3_{H_2})(X_{CH_4} X_{H_2O})/X^3_{H_2}(1/P^2) , \quad (5)$$

$$X_{CO_2} = K_6(\phi_{CH_4} \phi^2_{H_2O})/(\phi_{CO_2} \phi^4_{H_2})(X_{CH_4} X^2_{H_2O})/X^4_{H_2}(1/P^2) , \quad (6)$$

$$X_{HCN} = K_7(\phi_{CH_4} \phi_{NH_3})/(\phi_{HCN} \phi^3_{H_2})(X_{CH_4} X_{NH_3})/X^3_{H_2}(1/P^2) , \quad (7)$$

$$X_{PH_3} = [(1/K_8)(\phi_{P_4O_6} \phi^{12}_{H_2})/(\phi^4_{PH_3} \phi^6_{H_2O}) \times (X_{P_4O_6} X^{12}_{H_2}/X^6_{H_2O})P^3]^{1/4} , \quad (8)$$

$$X_{GeH_4} = K_9(\phi_{GeS} \phi^3_{H_2})/(\phi_{GeH_4} \phi_{H_2S})(X_{GeS} X^3_{H_2}/X_{H_2S})P^2 , \quad (9)$$

where K_n, the equilibrium constant for equation (n), is calculated from data in the JANAF tables and supplements and P, the total pressure, is calculated from

$$P \approx P_{H_2}/X_{H_2} , \quad (10)$$

taking P_{H_2} from the real H_2(g) adiabat in Figure 1. The fugacity coefficients (ϕ_i) in equations (4)–(9) were estimated using the Lewis fugacity rule (Prausnitz 1969),

$$\phi_i(\text{mixture}, T, P) = \phi_i(\text{pure}, T, P) , \quad (11)$$

and generalized fugacity coefficient tables and charts (Breedveld and Prausnitz 1973; Hougen, Watson, and Ragatz 1964; Newton 1935). Detailed explanations of the use of the generalized fugacity coefficient tables and charts, which are standard chemical engineering tools, are given elsewhere (e.g., Hougen, Watson, and Ragatz 1964; Breedveld and Prausnitz 1973; Reid, Prausnitz, and Sherwood 1977; Newton 1935) and will not be repeated here. However, these charts and tables require the use of the reduced parameters $T_R = T/T_C$ and $P_R = P/P_C$, where T_C, P_C are the critical parameters. Critical parameters for all gases involved in equations (4)–(9), except for P_4O_6, GeH_4, and GeS, were taken from standard sources or were calculated as described by Breedveld and Prausnitz (1973) for H_2, H_2O, and NH_3. The critical parameters for P_4O_6, GeH_4, and GeS were estimated using relations in Partington (1949, pp. 646–654), and auxiliary data from Thorpe and Tutton (1890), Kelley (1935), Glushko *et al.* (1978–1982), and *Matheson Gas Data Book* (1967).

The real gas thermochemical equilibrium abundances of several trace gases are displayed in Figure 6. These were calculated using equations (4)–(11), the fugacity coefficients discussed above, and our standard methods (e.g., see Barshay and Lewis 1978). Both the fugacity coefficient corrections (as functions of temperature and total pressure) and the incompressibility corrections are required to calculate properly real gas behavior in Uranus's deep atmosphere. For example, Figure 6 shows that the real gas mixing ratios for N_2, CO, CO_2, and HCN are all less than the ideal gas mixing ratios, while the reverse is true for PH_3 and GeH_4. However, consideration of only the incompressibility effects in equations (4)–(9) leads to the opposite (incorrect) result that the real gas N_2, CO, CO_2, HCN abundances are greater than the ideal gas values, while the real gas PH_3 and GeH_4 abundances are smaller than the ideal gas values.

Finally, we note that similar considerations apply to C_2H_6, where the relevant equation is

$$X_{C_2H_6} = K_{12}(\phi^2_{CH_4}/\phi_{C_2H_6} \phi_{H_2})(X^2_{CH_4}/X_{H_2}) . \quad (12)$$

The C_2H_6 mixing ratio is pressure independent, but the real gas C_2H_6 mixing ratios are also smaller than the ideal gas values (see Figs. 2 and 6).

V. THERMOCHEMICAL KINETICS AND UPWARD MIXING OF TRACE GASES

The results in Figures 2–5 show that N_2 in particular but also C_2H_6, CO, CO_2, CH_3OH, CH_3NH_2, HCN, PH_3, GeH_4, H_2Se, HCl, HF, and CH_3SH have significant abundances in the deep atmosphere. The thermochemical equilibrium abundances of all these species are, however, negligible in the upper troposphere on Uranus. However, CO, PH_3, and GeH_4 have been observed on Jupiter (Beer and Taylor 1978; Fink, Larson, and Treffers 1978; Larson *et al.* 1977, 1978; Kunde *et al.* 1982), and PH_3 has been observed on Saturn (Larson *et al.* 1980;

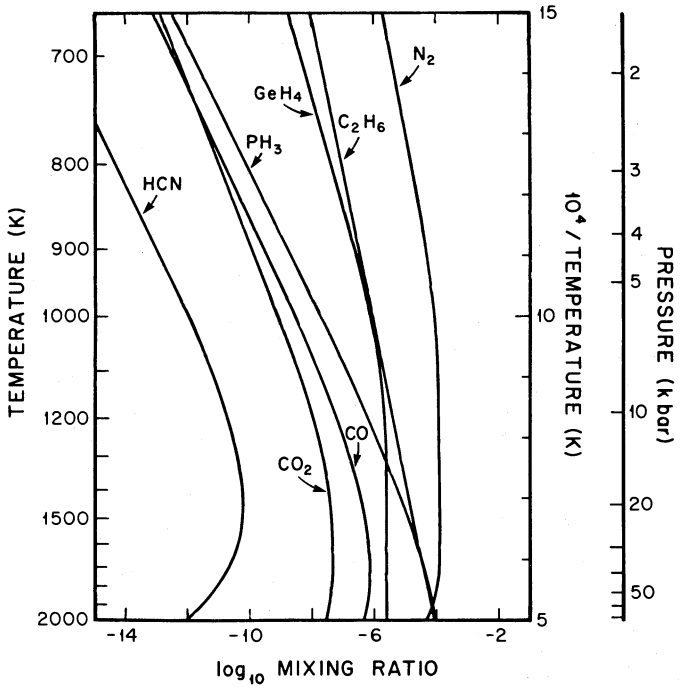

FIG. 6.—Real gas thermochemical equilibrium abundances for potential chemical probes of Uranus's deep atmosphere. The pressure scale is for a real gas adiabat. See text for details.

Courtin *et al.* 1984) at concentrations orders of magnitude greater than their thermochemical equilibrium values in the cool, visible regions of these two planetary atmospheres. For example, the observed GeH_4 mixing ratio on Jupiter ($X_{GeH_4} \approx 7 \times 10^{-10}$) and the observed PH_3 mixing ratio on Saturn ($X_{PH_3} \approx 0.2\text{–}2 \times 10^{-6}$) are 11 and 32–33 orders of magnitude, respectively, greater than the predicted thermochemical equilibrium mixing ratios (Fegley and Lewis 1979; Fegley and Prinn 1985*b*). These observations are direct evidence for the existence of a potent disequilibrating mechanism, namely, rapid vertical mixing on Jupiter and Saturn. The same disequilibrating mechanism is present on Uranus.

Despite the apparent absence of a significant internal heat source on Uranus, free convection theory suggests that fairly rapid vertical mixing may still occur in the deep atmosphere. Assuming that free convection is a dominant mode of vertical heat transport in the Uranian deep atmosphere, the relationship between the vertical eddy diffusion coefficient K and the upward heat flux ϕ carried by convection is

$$K \approx H(\phi/\rho\gamma)^{1/3}\,, \qquad (13)$$

where H is the pressure scale height, γ is C_p/R, and ρ is the atmospheric density. Taking H, γ, and ρ values appropriate for the 1000 K level in our atmospheric models and heat fluxes of 10–100 ergs cm^{-2} s^{-1}, we estimate vertical eddy diffusion coefficients of $K \approx 5 \times 10^7$–10^8 cm^2 s^{-1}. The lower heat flux of $\sim$10 ergs cm^{-2} s^{-1} is Danielson's (1977) estimate of radioactive heating from chondritic material in the core, and the upper heat flux of $\sim$100 ergs cm^{-2} s^{-1} is Hubbard's (1978) estimate of remaining primordial heat escaping from Uranus. The estimated K values suggest more sluggish convective mixing on Uranus than on Jupiter or Saturn where K values of $\sim 10^8$–10^9 cm^2 s^{-1} appear appropriate for the deep atmospheres (Stone 1976; Flasar and Gierasch 1977; Prinn *et al.* 1984).

In order to explore the possibility that convective mixing in the Uranian deep atmosphere may provide observable concentrations of N_2 and other chemical probes in the visible atmosphere we will examine the thermochemical kinetics of the reactions involved in the destruction and formation of N_2, CO, CO_2, HCN, PH_3, and GeH_4.

Prinn and Barshay (1977), Prinn and Olaguer (1981), and Fegley and Prinn (1985*b*) described a simple chemical-dynamical model to predict nonequilibrium trace gas abundances due to rapid vertical mixing in the atmospheres of Jupiter and Saturn. Fegley and Prinn (1985*a*) first quantitatively applied this model to Uranus, and here we greatly extend their results and consider real gas effects on the abundances of potential chemical probes of Uranus's deep atmosphere. Detailed descriptions of the thermochemical kinetic model are given in the papers above dealing with Jupiter and Saturn.

Briefly, we compare the time constant t_{chem} for the fastest reactions producing and destroying a gas to the time constant t_{conv} for convectively transporting the gas to a cooler region higher up in the atmosphere where these reactions will be kinetically inhibited. Following Prinn and Barshay (1977), we define the altitude $Z = Z^*$ at which $t_{chem} = t_{conv}$ as the quench level for a particular gas. This level is different for each gas studied and is therefore associated with a different quench temperature $T = T_Q$ for each gas. Although the quench temperatures for a particular gas fall within a fairly narrow range of $\sim$200 K from planet to planet (e.g., see Fegley and Prinn 1985*a*, *b*), they *must* be explicitly calculated for each planetary atmosphere model considered in order to avoid potentially serious errors in the predicted trace gas mixing ratios. For example, the calculated CO quench temperatures for homogeneous gas-phase destruction of CO are 1070 K on Jupiter and 970 K on Saturn (Fegley and Prinn 1985*b*). Although these values differ by only 100 K, taking the Saturn T_Q value for CO destruction on Jupiter yields a predicted CO mixing ratio 10 times smaller than the observed value. However, the observed CO mixing ratio on Jupiter is matched by the predicted value at $T_Q = 1070$ K (Prinn and Barshay 1977; Fegley and Prinn 1985*b*). Significant errors in predicted mixing ratios for nonequilibrium trace gases on Uranus may also result if quench temperatures are assumed by analogy with other planets (e.g., Jupiter, Saturn) rather than being explicitly calculated.

In the present work we calculate T_Q by computing the level Z^*, where $t_{chem} = t_{conv} \approx H^2/K$, H is the pressure scale height, and K is the vertical eddy diffusion coefficient. We vary K over a wide range to predict nonequilibrium trace gas abundances for different assumed degrees of convective vertical transport. The assumed rate-determining reactions which we use to calculate the t_{chem} values for N_2, CO, CO_2, HCN, PH_3, and GeH_4 and the homogeneous gas-phase rate constants are listed in Table 4. These reactions and rate constants are taken from our previous papers which provide thorough discussions of them (Fegley and Prinn 1985*b*; Prinn and Fegley 1981; Prinn and Olaguer 1981; Prinn and Barshay 1977; Lewis and Prinn 1980).

Figure 7 displays the predicted N_2, CO, CO_2, HCN, PH_3, and GeH_4 mixing ratios in the observable Uranian atmosphere for a wide range of assumed vertical eddy diffusion coefficients. Results are shown for both the ideal gas (Figs. 2–5) and real gas (Fig. 6) abundance profiles. Predicted mixing ratios at K values of 10^7–10^8 cm^2 s^{-1} (shaded region in Fig. 7), appropriate for assumed heat fluxes of 10–100 ergs cm^{-2} s^{-1}, are given in Table 5. Dissolution of these species in the water

TABLE 4

REACTIONS AND RATE CONSTANTS USED TO ESTIMATE t_{chem} VALUES FOR NONEQUILIBRIUM TRACE GASES

Number	Reaction	Rate Constant
1.....	$N_2 + H_2 \rightarrow NH + NH$	$8.45 \times 10^{-8} \exp(-81{,}515/T)$
2.....	$CH_2O + H_2 \rightarrow CH_3 + OH$	$2.3 \times 10^{-10} \exp(-36{,}200/T)$
3.....	$CO + OH \rightarrow CO_2 + H$	$1.1 \times 10^{-13} \exp(0.0009T)$
4.....	$HCN + H_2 \rightarrow CH_2 + NH$	$1.08 \times 10^{-8} \exp(-70{,}456/T)$
5.....	$PH + OH \rightarrow PO + H_2$	10^{-9}
6.....	$GeH + SH \rightarrow GeS + H_2$	10^{-9}

NOTE.—Units for two- body rate constants are $cm^3\ s^{-1}$.

clouds and condensation of these species in the very cool visible atmosphere will serve to decrease somewhat the observed mixing ratios from those tabulated.

The results in Figure 7 and Table 5 illustrate several important points. First, N_2 is predicted to be the most abundant nonequilibrium trace gas derived from the deep atmosphere. PH_3 is predicted to be more abundant than N_2 only for $K > 10^{15}$ $cm^2\ s^{-1}$ in the real gas case. However, PH_3 may be more soluble than N_2 in the aqueous solution clouds and therefore may be relatively more depleted in the upper atmosphere above the water clouds. The calculated Henry's law constants are $\sim 6.8 \times 10^3$ bars for PH_3 and $\sim 8.5 \times 10^4$ bars for N_2 at 298 K (Wagman *et al.* 1968), which supports this suggestion. In any case, vertical eddy diffusion coefficients $K \geq 10^{15}$ $cm^2\ s^{-1}$ are totally incompatible with the observational upper limits on internal heat fluxes (Orton and Appleby 1984; Moseley, Conrath, and Silverberg 1985) and are thus unrealistic. Second, the N_2, HCN, CO and CO_2 mixing ratios for the real gas case are all smaller than those for the ideal gas case at all K values from 10^0 to 10^{15} $cm^2\ s^{-1}$. Last, the PH_3 and GeH_4 mixing ratios are larger in the real gas case for all K values studied.

The abundances of all these potential chemical probes (except N_2 and CO) are severely limited by their saturation vapor pressures in the cold Uranian upper atmosphere. Based on extrapolations of the vapor pressure data for HCN(s), CO_2(s), and GeH_4(liq) in Stull (1947) and for PH_3(s) in Stephenson and Giauque (1937), the estimated mixing ratios at the 74 K, 1 bar level are $\sim 10^{-20}$ (HCN), $\sim 10^{-12}$ (CO_2), $\sim 10^{-7}$ (PH_3), and $\leq 10^{-6}$ (GeH_4). Only PH_3, GeH_4, N_2, and CO

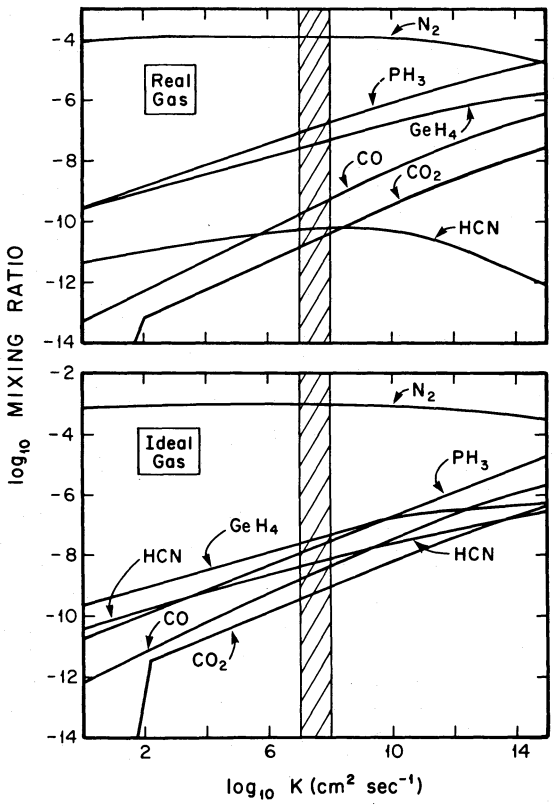

FIG. 7.—Predicted mixing ratios of chemical probes in the observable Uranian atmosphere as a function of the vertical eddy diffusion coefficient K. Both real gas and ideal gas calculations are displayed. Shaded region at $K = 10^7$–10^8 $cm^2\ s^{-1}$ is appropriate for assumed convective heat fluxes of 10–100 ergs $cm^{-2}\ s^{-1}$. Kinks in the two CO_2 curves occur at the aqueous solution cloud base of ~ 647 K. Only homogeneous gas-phase reactions are plotted. See text for details.

appear to be potentially observable in the cold upper atmosphere. An *upper limit* of $\sim 5 \times 10^{-6}$ for the CO mixing ratio was recently reported by deBergh, Lutz, and Owen (1985). However, this upper limit does not allow us to test the validity of our predictions since it is $\sim 10^3$–10^4 times larger than the CO mixing ratio predicted by vertical mixing at $K = 10^7$–10^8

TABLE 5

PREDICTED MIXING RATIOS OF CHEMICAL PROBES ON URANUS[a,b]

	Real Gas		Ideal Gas	
Probe	Quench Temperature (K)	Mixing Ratio	Quench Temperature (K)	Mixing Ratio
N_2	1538–1578[c]	1.3×10^{-4}	1469–1526	$(9.0–10) \times 10^{-4}$
PH_3.....	1070–1120	$0.9–2.0 \times 10^{-7}$	1059–1102	$(0.11–0.28) \times 10^{-7}$
GeH_4	778–811	$2.6–5.4 \times 10^{-8}$	771–803	$(2.5–4.8) \times 10^{-8}$
HCN	1371–1431	$5.6–6.3 \times 10^{-11}$	1332–1387	$(4.2–7.8) \times 10^{-9}$
CO.....	885–931[c]	$1.8–6.0 \times 10^{-10}$	874–917	$(1.6–4.6) \times 10^{-9}$
CO_2	808–850	$1.4–3.7 \times 10^{-11}$	794–836	$(4.0–11) \times 10^{-10}$

[a] Predictions assume 500 times solar composition and $K = 10^7$–10^8 $cm^2\ s^{-1}$.

[b] Condensation in the cold upper atmosphere will significantly decrease HCN and CO_2 mixing ratios from those tabulated (see text). Dissolution in the water clouds will decrease the tabulated mixing ratios of all species but not by a large amount.

[c] Homogeneous gas-phase reactions only are considered because the presence of Fe particles in the deep atmosphere is very unlikely. Heterogeneous reactions considered in Fegley and Prinn 1985*a*.

$cm^2\ s^{-1}$ and is in fact larger than any CO mixing ratio which can be produced solely by rapid vertical mixing (see Fig. 7). The only other *upper limit* on a nonequilibrium trace gas of which we are aware is $\sim 3 \times 10^{-7}$ for the CH_3NH_2 mixing ratio (Fink and Larson 1979). No kinetic data are available for thermochemical reactions involving CH_3NH_2 so a quench level cannot be calculated, but the ideal gas calculations show that the reported upper limit corresponds to the $T \approx 1200$ K level.

The N_2 mixing ratio is of particular interest because N_2 is potentially the most abundant nonequilibrium gas in the tropospheres of Jupiter, Saturn, and Uranus (Prinn and Olaguer 1981; Fegley and Prinn 1985*a*, *b*; Stevenson 1984). Table 6 compares the predicted N_2 mixing ratios for a suite of compositional models enriched from 10 to 500 times in ice- and rock-forming elements (applicable to cases 1 and 3 in Tables 1 and 2). The predicted N_2 mixing ratios increase from ~ 1 ppmv (10 times solar) to ~ 1000 ppmv (500 times solar) in the ideal gas case. However, the real gas values in the range of ~ 0.2–130 ppmv (10–500 times solar) are more realistic predictions.

Compositional models enriched more than 500 times with respect to solar abundances are not compatible with the observed CH_4/H_2 mixing ratio and the independently estimated gas/solid ratio, unless nitrogen and carbon were primarily in the form of N_2 and CO when Uranus formed (see the kinetic inhibition models in Tables 1 and 2). However, the arguments against large N_2 mixing ratios much greater than 130 ppmv are even more compelling for these kinetic inhibition models because less nitrogen is incorporated into the planet to begin with. Equation (4) shows that X_{N_2} is proportional to $X^2_{NH_3}$, and NH_3 is the dominant nitrogen- bearing gas for all plausible Uranus atmosphere models (see Fig. 1). Therefore small decreases in the planetary nitrogen inventory have a large impact on the N_2 mixing ratio. For example, the preferred kinetic inhibition model (case 4,1000 times enriched) has condensate $N_2 > NH_3$ but also has ~ 10 times less total nitrogen to start with than the model shown in Figures 2–7, and consequently the calculated N_2 mixing ratios are ~ 100 times smaller.

Furthermore, consideration of heterogeneous iron-catalyzed reactions for $N_2 + H_2$ leads to still smaller N_2 mixing ratios.

TABLE 6

PREDICTED N_2 MIXING RATIOS[a] FOR $K = 10^7$–10^8 $cm^2\ s^{-1}$

Enrichment Factor	Quench Temperature (K)	Mixing Ratio
10.....	1425–1481	$(1.3–1.5) \times 10^{-6}$
	1452–1510[b]	$(2.4–2.5) \times 10^{-7}$
50.....	1435–1492	$(2.6–2.7) \times 10^{-5}$
	1466–1524[b]	$(5.5–5.8) \times 10^{-6}$
100[c].....	1440–1496	$(7.0–7.4) \times 10^{-5}$
	1477–1537[b]	$(1.6–1.7) \times 10^{-5}$
500.....	1469–1526	$(9.0–10) \times 10^{-4}$
	1538–1578[b]	1.3×10^{-4}

[a] As a function of assumed enrichment over solar composition abundances. Predictions are for the case 3 generic models (see Tables 1 and 2) and are for homogeneous gas-phase reactions.

[b] Real gas calculations including fugacity coefficients as $f(P, T)$ and incompressibility effects.

[c] See Fegley and Prinn 1985*a* for a description of this model.

Fegley and Prinn (1985*a*) used the method of Prinn and Olaguer (1981) to model heterogeneous iron-catalyzed $N_2 + H_2$ reactions in a 100 times enriched Uranus model. They found that lower N_2 mixing ratios of $(5.0–6.3) \times 10^{-5}$ (vs. $[7.0–7.4] \times 10^{-5}$ for homogeneous gas-phase reactions) resulted for eddy diffusion coefficients of 10^7–10^8 $cm^2\ s^{-1}$. Larger eddy diffusion coefficients gave comparable or greater decreases for the iron-catalyzed reactions.

Finally, as Figure 7 illustrates, larger assumed vertical eddy diffusion coefficients yield approximately the same N_2 mixing ratios in the ideal gas case and smaller mixing ratios in the real gas case. Thus more rapid vertical mixing will not supply more N_2.

Taken together, all these arguments strongly suggest that N_2 mixing ratios of ~ 130 ppmv are the *maximum* to be expected in the troposphere of Uranus. The inferred depletion of NH_3 in the 150–200 K region (de Pater and Massie 1985; Gulkis, Janssen, and Olsen 1978; Gulkis *et al.* 1983; Klein and Turegano 1978; Fink and Larson 1979) also suggests that N_2 production by NH_3 photolysis is likely to be negligible. Thus, vertical mixing is predicted to be the major source of N_2 in the troposphere of Uranus.

VI. CONDENSATION OF AQUEOUS SOLUTION CLOUDS AND THEIR EFFECTS ON ATMOSPHERIC DYNAMICS AND PHYSICS

a) Water Vapor Profiles

Three qualitatively different types of water vapor profiles were found for the Uranus atmosphere models which we studied. Figure 8 illustrates the three types of behavior, which correspond to subcritical, critical, and supercritical formation of the aqueous solution clouds. As Figure 1 shows, aqueous solution clouds will form at higher temperatures as the H_2O abundance increases until the pure H_2O critical temperature of 647 K is reached. This type of subcritical behavior is shown in Figure 8 where the intersection of a H_2O abundance line with the water vapor profile curve gives the corresponding cloud base temperature, e.g., ~ 400 K for the 10 times solar model shown. For comparison, Atreya and Romani (1985), Hunten (1984), and Weidenschilling and Lewis (1973) give the aqueous solution cloud base temperature for a 10 times solar composition model as ~ 420 K, ~ 400 K, and ~ 390 K, respectively. The small differences in these results are in large part due to the slightly different (P, T) profiles used. This is also shown in Figure 8; the water vapor profiles for the three cases illustrated are shifted slightly because of the different total pressures at a given temperature. Our calculated cloud base temperatures for H_2O mixing ratios of 2% (448 K) and 3% (483 K) also agree well with Hunten's (1984) values of ~ 438 K and ~ 470 K, respectively. Again, slightly different (P, T) profiles account for most of the differences.

This type of subcritical behavior continues until a H_2O mixing ratio corresponding exactly to a cloud base temperature of 647 K is reached. At this critical mixing ratio there is *no* discontinuity in the water vapor profile due to formation of aqueous solution clouds. This critical behavior is displayed by the 120 times solar composition curve in Figure 8. Larger H_2O mixing ratios now result in a third kind of qualitatively different behavior. Because larger enrichments of the H_2O abundance over solar composition can no longer produce aqueous solution condensation at higher temperatures than 647 K, large sudden decreases in the H_2O mixing ratio now occur associated with the onset of solution condensation at 647

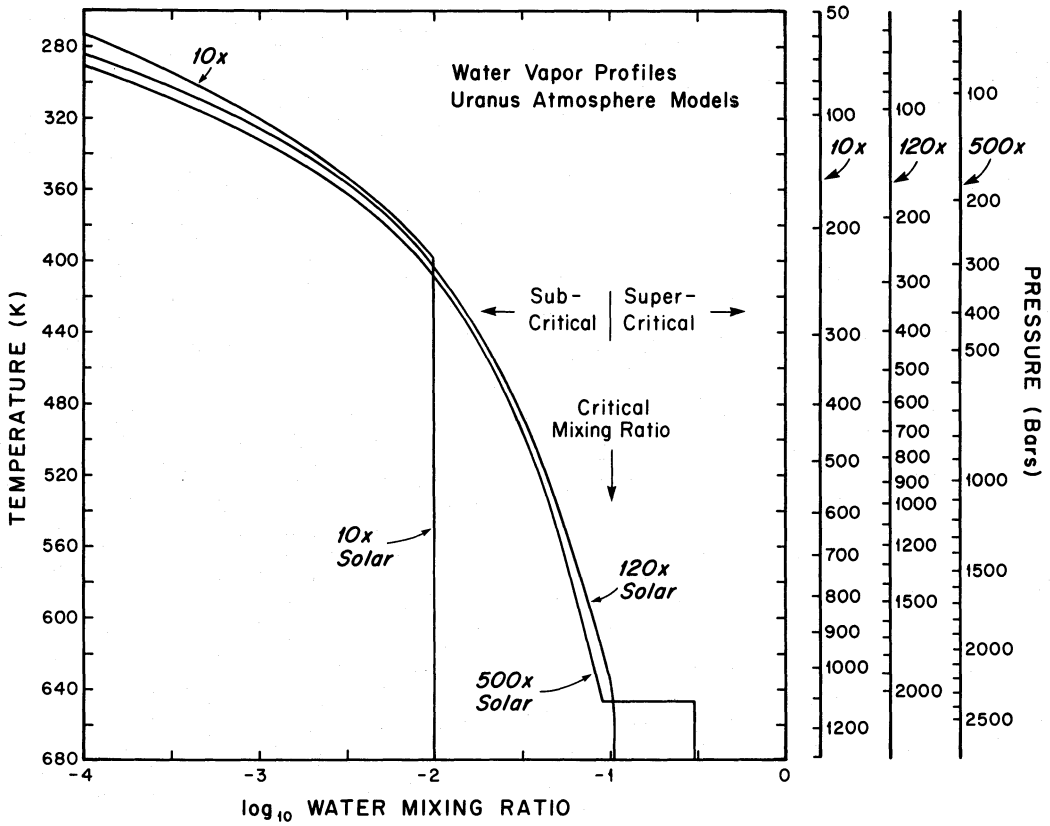

FIG. 8.—Predicted water vapor profiles for our Uranus atmosphere models. Three qualitatively different types of behavior are illustrated for subcritical, critical, and supercritical formation of the aqueous solution clouds. Three pressure scales (wet lapse rates) on the vertical axis were calculated using eq. (3) and correspond to the 10, 120, and 500 times solar models shown.

K. Abrupt discontinuities will thus result in both the H_2O vapor abundance profile and in the abundances of soluble species when cloud formation occurs. This supercritical behavior is displayed by the 500 times solar composition model in Figure 8 and was also shown in Figures 2–6. These conclusions are not qualitatively changed by considering the increase in H_2O(liq) thermodynamic activity with pressure (Poynting effect), the decrease in H_2O(liq) activity with dissolved solutes, and the fugacity coefficients for real H_2O gas because these effects tend to cancel one another.

b) *Consequences of Critical and Supercritical Behavior*

Several potentially important consequences may result from the critical and supercritical behavior described above. These will only be listed because their complete consideration is beyond the scope of the present paper. First, the heat of vaporization for the liquid → vapor phase change goes to zero at the critical point as the distinction between the two phases vanishes (Keenan *et al.* 1969; Levelt-Sengers 1977). In this case the wet and dry lapse rates will be identical. This is easily seen by considering the equation for the wet lapse rate given by Lewis (1969*b*)

$$(\partial T/\partial z)_s = -\bar{\mu}g/[C_p + (\Delta H_{vap})X_w(\Delta H_{vap}/RT^2 - 1/T)] , \quad (14)$$

where $\bar{\mu}$ is the mean molecular weight of atmospheric gas and X_w is the water vapor mixing ratio. As $\Delta H_{vap} \to 0$, then $(\partial T/\partial z)_s \to -\bar{\mu}g/C_p$. Second, other thermodynamic properties (e.g., the isothermal compressibility β_T, the heat capacities at constant pressure C_p and constant volume C_v, the isobaric thermal expansion coefficient α_p, the sound speed), transport properties (e.g., the viscosity and thermal conductivity), and dimensionless numbers which describe fluid flow (e.g., the Rayleigh and Prandtl numbers) all show anomalies at the critical point (Levelt-Sengers 1977). The large increases in the Rayleigh number, which occur at the critical point, may greatly increase the tendency toward convection (Levelt-Sengers 1977). Third, the condensation of a significant fraction of the available H_2O at the critical point will suddenly alter the mean molecular weight $\bar{\mu}$ of the atmosphere. This sudden decrease in $\bar{\mu}$ and in the mean atmospheric density $\bar{\rho}$ will result in a large upward buoyancy force and acceleration given by

$$F_{buo} \approx g(\bar{\rho}_{amb} - \bar{\rho}_{mov}) , \quad (15)$$

$$\partial^2 z/\partial t^2 \approx g[(\bar{\mu}_{amb}/\bar{\mu}_{mov}) - 1] , \quad (16)$$

where the subscripts "amb" and "mov" refer to the ambient and moving atmospheric parcels (i.e., before and after H_2O condensation occurs). For the 500 times solar model studied in this paper, $\Delta\bar{\rho} \approx 0.2$ g cm^{-3} and $\bar{\mu}_{amb}/\bar{\mu}_{mov} \approx 1.8$, giving an upward buoyancy acceleration of ~ 0.8 g! Thus, qualitatively both the increased Rayleigh number and the decreased $\bar{\mu}$ indicate greatly enhanced vertical transport immediately at the critical point (647 K) but without any latent heat effects due to the condensation of the aqueous solution clouds!

We previously noted that the solubility of CH_4, NH_3, and H_2 in the aqueous solution clouds will slightly decrease (NH_3, CH_4) or slightly increase (H_2) the H_2O critical point. However, the presence of these solutes does not alter our conclusions above because multicomponent fluids show analogous anom-

alies in their critical region behavior (Levelt-Sengers 1977). At present the exact behavior of the H_2O critical point in the H_2O–H_2–He–CH_4–NH_3 system is difficult to predict because of the lack of experimental data on the He–H_2O binary and on the five-component system. However, the existing data (Tsiklis, Linshits, and Goryunova 1965; DeLoos, Wijen, and Diepen 1980; Seward and Franck 1981) do *not* suggest critical temperatures very much greater than 647 K.

Finally, we note that supercritical H_2O is a highly corrosive solvent which dissolves many inorganic compounds including rock-forming minerals. For example, the solubility of quartz (SiO_2) in supercritical water reaches $\sim$750 g per 1 kilogram of fluid at the upper critical endpoint of $\sim$1353 K and 9.7 kb where SiO_2–fluid-melt are in equilibrium (Kennedy *et al.* 1962). More complex minerals [e.g., $MgSiO_3$, $NaAlSi_3O_8$, $CaCO_3$, $CaMg(CO_3)_2$, $CaSO_4$, etc.] also readily dissolve in supercritical water (Morey 1957; Holland and Malinin 1979). These qualitative considerations suggest that infalling rocky planetesimals and the "core" of Uranus are soluble (at least to a limited extent) in the "atmosphere." Stevenson (1982*b*) has made qualitatively similar observations.

VII. CONCLUDING REMARKS

The results of our generic planetary modeling, the thermochemical equilibrium calculations, and cloud condensation models confirm our initial statement that the deep atmosphere of Uranus is fundamentally different from the atmospheres of Jupiter and Saturn. All generic planetary models considered require that ice- and rock-forming elements be enriched between 100 to 1000 times above their solar composition abundances. Such large enrichments suggest that the deep atmosphere is a H_2O–rich supercritical fluid with the formation of aqueous solution clouds occurring at high temperatures and great depth in the atmosphere. These clouds are constrained to form at $T \leq 647$ K by the phase relations for pure H_2O and the CH_4–H_2O, H_2–H_2O, and NH_3–H_2O systems. The abundances of several species in the atmosphere above the water clouds (notably NH_3 and CH_4) are reduced appreciably by the solution of these gases in the clouds. The solubility of NH_3 in the water clouds and its effects for the NH_3/H_2 mixing ratio in the atmosphere of Uranus were first noted by Atreya (1983) and later confirmed by several authors (Atreya 1984; Atreya and Romani 1985; Stevenson 1984; Fegley and Prinn 1985*a*). The generic planetary models considered also imply that formation of Uranus from large reservoirs of disequilibrium C and N as first suggested by Lewis and Prinn (1980) may (measurably) deplete H_2 and increase the He/H_2 ratio in the visible Uranus atmosphere.

Thermochemical equilibrium and kinetic calculations for a wide range of atmosphere models also predict that N_2 is the most abundant nonequilibrium trace species mixed upward from the deep atmosphere of Uranus. Other less abundant species predicted to be mixed upward from the deep atmosphere are PH_3, GeH_4, CO, CO_2, and HCN. Other potential chemical probes such as C_2H_6, CH_3OH, CH_3NH_2, H_2Se, HCl, HF, and CH_3SH were also identified, but no kinetic data are available to make quantitative predictions. Furthermore, our best estimates of their solubilities in the aqueous solution clouds suggest that many of these species can readily dissolve in the (hypothesized) clouds.

Because thermal radiance observations suggest that the deep atmosphere of Uranus is much colder and denser than the atmospheres of Jupiter and Saturn (i.e., greater pressure at a given temperature), we have carefully studied the effects of nonideal gas behavior on the abundances of these potential chemical probes and on the N_2 abundance in particular. These studies include the effects of deviations from the ideal gas law (incompressibility effects) and *more importantly* the variation of gas fugacity coefficients with both temperature and pressure. The results predict that the abundances of N_2, CO, CO_2, and HCN are reduced by real gas effects, while the abundances of PH_3 and GeH_4 are increased. Consideration of the incompressibility effects alone leads to the incorrect conclusion that the opposite behavior occurs, i.e., N_2, CO, CO_2, and HCN increase, while PH_3 and GeH_4 decrease.

Quantitative calculation of the N_2 mixing ratio due to vertical transport from the deep atmosphere shows that N_2 mixing ratios of $\sim$130 ppmv are the maximum to be expected in the troposphere of Uranus. This conclusion is valid for all compositional models which agree with observed constraints on the chemistry of Uranus, and it is consistent with the observed upper limits on the internal heat flux.

Finally, for H_2O mixing ratios exceeding $\sim$120 times solar, abrupt condensation at the critical point leads to dynamical instabilities (e.g., large upward buoyancy accelerations caused by the drop in average atmospheric molecular weight) which are expected to enhance greatly vertical mixing at this point but without latent heat effects. This behavior is markedly different from those familiar in water condensation on Earth.

This work was supported by NSF grant ATM-84-01232 to MIT. We thank E. Bettez for assisting with programming while working in the MIT UROP Program, J. Sloman for preparing the manuscript, and D. Souza for drafting the figures.

REFERENCES

Atreya, S. K. 1983, unpublished.
———. 1984, in *Uranus and Neptune*, ed. J. T. Bergstralh (NASA CP2330), p. 55.
Atreya, S. K., and Romani, P. N. 1985, in *Recent Advances in Planetary Meteorology*, ed. G. E. Hunt (Cambridge: Cambridge University Press), p. 17.
Baines, K. H. 1983, *Icarus*, **56**, 543.
Barshay, S. S., and Lewis, J. S. 1976, *Ann. Rev. Astr. Ap.*, **14**, 81.
———. 1978, *Icarus*, **33**, 593.
Beer, R., and Taylor, F. W. 1978, *Ap. J.*, **221**, 1100.
Bergstralh, J. T., and Baines, K. H. 1984, in *Uranus and Neptune*, ed. J. T. Bergstralh (NASA CP2330), p. 179.
Breedveld, G. J. F., and Prausnitz, J. M. 1973, *Am. Institution Chem. Eng. J.*, **19**, 783.
Cameron, A. G. W. 1978*a*, in *The Origin of the Solar System*, ed. S. F. Dermott (New York: Wiley), p. 49.
———. 1978*b*, in *Protostars and Planets*, ed. T. Gehrels (Tucson: University of Arizona Press), p. 453.
Cameron, A. G. W. 1982, in *Essays in Nuclear Astrophysics*, ed. C. A. Barnes, D. D. Clayton, and D. N. Schramm (Cambridge: Cambridge University Press), p. 23.
Chase, M. W., Curnutt, J. L., Hu, A. T., Prophet, H., Syverud, A. N., Walker, L. C., Downey, J. R., Jr., McDonald, R. A., and Valenzuela, E. A., eds. 1971–1985, *JANAF SUPPL.* (Midland, MI: Dow Chemical Co.).
Clever, H. L., and Han, C. H. 1980, in *Thermodynamics of Aqueous Systems with Industrial Applications*, ed. S. A. Newman, H. E. Barnes, M. Klein, and S. J. Sandler (Washington, DC: American Chemical Society), p. 513.
Courtin, R., Gautier, D., Marten, A., Bezard, B., and Hanel, R. 1984, *Ap. J.*, **287**, 899.
Culberson, O. L., and McKetta, J. J., Jr. 1951, *Trans. Am. Institution Mech. Eng.*, **192**, 223.
Danielson, R. E. 1977, *Icarus*, **30**, 462.
deBergh, C., Lutz, B. L., and Owen, T. 1985, *Bull. AAS*, **17**, 743.
DeLoos, Th. W., Wijen, A. J. M., and Diepen, G. A. M. 1980, *J. Chem. Thermodynamics*, **12**, 193.

de Pater, I., and Massie, S. T. 1985, *Icarus*, **62**, 143.
Fazio, G. G., Traub, W. A., Wright, E. L., and Low, F. J. 1976, *Ap. J.*, **209**, 633.
Fegley, B., Jr., and Lewis, J. S. 1979, *Icarus*, **38**, 166.
———. 1980, *Icarus*, **41**, 439.
Fegley, B., Jr., and Prinn, R. G. 1985*a*, *Nature*, **318**, 48.
———. 1985*b*, *Ap. J.*, **299**, 1067.
Fink, U., and Larson, H. P. 1979, *Ap. J.*, **233**, 1021.
Fink, U., Larson, H. P., and Treffers, R. R. 1978, *Icarus*, **34**, 344.
Flasar, M., and Gierasch, P. 1977, in *Proc. Symposium on Planetary Atmospheres*, ed. A. Vallance-Jones (Ottawa: Royal Society of Canada), p. 85.
Glushko, V. P., Gurvich, L. V., Bergman, G. A., Veitz, I. V., Medvedev, V. A., Khachkuruzov, G. A., and Yungman, V. S., eds. 1978–1982, *Thermodynamic Properties of Individual Substances*, Vols. **1–4**, (Moscow: High-Temperature Institute).
Gulkis, S., and de Pater, I. 1984, in *Uranus and Neptune*, ed. J. T. Bergstralh (NASA CP2330), p. 225.
Gulkis, S., Janssen, M. A., and Olsen, E. T. 1978, *Icarus*, **34**, 10.
Gulkis, S., Olsen, E. T., Klein, M. J., and Thompson, T. J. 1983, *Science*, **221**, 453.
Hayduk, W., and Laudie, W. 1973, *Am. Institution Chem. Eng. J.*, **19**, 1233.
Hess, S. L. 1959, *Introduction to Theoretical Meteorology* (New York: Holt, Rinehart, & Winston).
Holland, H. D., and Malinin, S. D. 1979, in *Geochemistry of Hydrothermal Ore Deposits*, ed. H. L. Barnes (New York: Wiley), p. 461.
Hougen, O. A., Watson, K. M., and Ragatz, R. A. 1964, *Chemical Process Principles*, Pt. II (New York: Wiley).
Hubbard, W. B. 1978, *Icarus*, **35**, 177.
———. 1984, in *Uranus and Neptune*, ed. J. T. Bergstralh (NASA CP2330), p. 291.
Hubbard, W. B., and MacFarlane, J. J. 1980, *J. Geophys. Res.*, **85**, 225.
Hunten, D. M. 1984, in *Uranus and Neptune*, ed. J. T. Bergstralh (NASA CP2330), p. 27.
Keenan, J. H., Keyes, F. G., Hill, P. G., and Moore, J. G. 1969, *Steam Tables* (New York: Wiley).
Kelley, K. K. 1935, *Contributions to the Data on Theoretical Metallurgy*, Vol. **3**, *The Free Energies of Vaporization and Vapor Pressures of Inorganic Substances* (Washington, DC: *US. Bureau Mines Bull.*, No. 383).
———. 1937, *Contributions to the Data on Theoretical Metallurgy*, Vol. **7**, *The Thermodynamic Properties of Sulphur and Its Inorganic Compounds* (Washington DC: *US Bureau Mines Bull.*, No. 406).
———. 1960, *Contributions to the Data on Theoretical Metallurgy*, Vol. **13**, *High-Temperature Heat-Content, Heat-Capacity, and Entropy Data for the Elements and Inorganic Compounds* (Washington, DC: *US Bureau Mines Bull.*, No. 584).
Kelley, K. K., and King, E. G. 1961, *Contributions to the Data on Theoretical Metallurgy*, Vol. **14**, *Entropies of the Elements and Inorganic Compounds* (Washington, DC: *US Bureau Mines Bull.*, No. 592).
Kennedy, G. C., Wasserburg, G. J., Heard, H. C., and Newton, R. C. 1962, *Am. J. Sci.*, **260**, 501.
Klein, M. J., and Turegano, J. A. 1978, *Ap. J.*, **224**, 431.
Kunde, V., *et al.* 1982, *Ap. J.*, **263**, 443.
Larimer, J. W. 1967, *Geochim. et Cosmochim. Acta*, **31**, 1215.
Larimer, J. W., and Anders, E. 1967, *Geochim. et Cosmochim. Acta*, **31**, 1239.
———. 1970, *Geochim. et Cosmochim. Acta*, **34**, 367.
Larsen, E. R., and Prausnitz, J. M. 1984, *Am. Institution Chem. Eng. J.*, **30**, 732.
Larson, H. P., Fink, U., Smith, H. A., and Davis, D. S. 1980, *Ap. J.*, **240**, 327.
Larson, H. P., Fink, U., and Treffers, R. R. 1978, *Ap. J.*, **219**, 1084.
Larson, H. P., Treffers, R. R., and Fink, U. 1977, *Ap. J.*, **211**, 972.
Lasker, B. M. 1963, *Ap. J.*, **138**, 709.
Levelt-Sengers, J. M. H. 1977, in *High Pressure Technology*, Vol. **2**, ed. I. L. Spain and J. Paauwe (New York: Marcel Dekker), p. 161.
Lewis, J. S. 1969*a*, *Icarus*, **10**, 393.
———. 1969*b*, *Icarus*, **10**, 365.
———. 1972*a*, *Icarus*, **16**, 241.
———. 1972*b*, *Earth Planet. Sci. Letters*, **15**, 286.
Lewis, J. S., and Prinn, R. G. 1980, *Ap. J.*, **238**, 357.
Leyko, J. 1964, *Bull. Acad. Polon. Sci. Ser. Chim.*, **12**, 275.
Lindal, G. F., *et al.* 1981, *J. Geophys. Res.*, **86**, 8721.
Loewenstein, R. F., Harper, D. A., Moseley, S. H., Telesco, C. M., and Thronson, H. A. 1977, *Icarus*, **31**, 315.
Lunine, J. I., and Stevenson, D. J. 1985, *Ap. J. Suppl.*, **58**, 493.
Matheson Gas Data Book. 1967 (4th ed.; East Rutherford, NJ: Matheson Co.).
Mills, R. L., Liebenberg, D. H., Bronson, J. C., and Schmidt, L. C. 1977, *J. Chem. Phys.*, **66**, 3076.
Mizuno, H. 1980, *Progr. Theor. Phys.*, **64**, 544.
Morey, G. W. 1957, *Econ. Geol.*, **52**, 225.
Moseley, H., Conrath, B., and Silverberg, R. F. 1985, *Ap. J. (Letters)*, **292**, L83.
Newton, R. H. 1935, *Industrial Eng. Chem.*, **27**, 302.
Orton, G. S., and Appleby, J. F. 1984, in *Uranus and Neptune*, ed. J. T. Bergstralh (NASA CP2330), p. 89.
Orton, G. S., Tokunaga, A. T., and Caldwell, J. 1983, *Icarus*, **56**, 147.
Partington, J. R. 1949, *An Advanced Treatise on Physical Chemistry*, Vol. **1**, (London: Longmans Green).
Perri, F., and Cameron, A. G. W. 1974, *Icarus*, **22**, 416.
Podolak, M., and Reynolds, R. T. 1984, *Icarus*, **57**, 102.
Prausnitz, J. M. 1969, *Molecular Thermodynamics of Fluid-Phase Equilibria* (Englewood Cliffs, NJ: Prentice Hall).
Price, L. C. 1979, *Am. Ass. Petrol. Geo. Bull.*, **63**, 1527.
Prinn, R. G. 1973, *Planet. Space Sci.*, **21**, 1601.
———. 1982, *Planet. Space Sci.*, **30**, 741.
Prinn, R. G., and Barshay, S. S. 1977, *Science*, **198**, 1031.
Prinn, R. G., and Fegley, B., Jr. 1981, *Ap. J.*, **249**, 308.
Prinn, R. G., Larson, H. P., Caldwell, J. J., and Gautier D., 1984, in *Saturn*, ed. T. Gehrels and M. S. Matthews (Tucson: University of Arizona Press), p. 88.
Prinn, R. G., and Lewis, J. S. 1973, *Ap. J.*, **179**, 333.
Prinn, R. G., and Olaguer, E. P. 1981, *J. Geophys. Res.*, **86**, 9895.
Reid, R. C., Prausnitz, J. M., and Sherwood, T. K. 1977, *The Properties of Gases and Liquids* (New York: McGraw-Hill).
Reynolds, R. T., and Summers, A. L. 1965, *J. Geophys. Res.*, **70**, 199.
Roberts, B. E., and Tremaine, P. R. 1985, *Canadian J. Chem. Eng.*, **63**, 294.
Rowlinson, J. S., and Swinton, F. L. 1982, *Liquids and Liquid Mixtures* (3d ed.; London: Butterworths).
Scatchard, G., Epstein, L. F., Warburton, J., Jr., and Cody, P. J. 1947, *Refrig. Eng.*, **53**, 413.
Seward, T. M., and Franck, E. W. 1981, *Ber. Bunsenges. Phys. Chem.*, **85**, 2.
Stephenson, C. C., and Giauque, W. F. 1937, *J. Chem. Phys.*, **5**, 149.
Stevenson, D. J. 1982*a*, *Ann. Rev. Earth Planet, Sci.*, **10**, 257.
———. 1982*b*, *Planet. Space Sci.*, **30**, 755.
———. 1984, *Bull. Am. Astr. Soc.*, **16**, 658.
Stone, P. H. 1976, in *Jupiter*, ed. T. Gehrels (Tucson: University of Arizona Press), p. 586.
Stull, D. R. 1947, *Industrial Eng. Chem.*, **39**, 517.
Stull, D. R., and Prophet, H. 1971, *JANAF Thermochemical Tables* (2nd ed.; NSRDS-NBS 37).
Stull, D. R., Westrum, E. F., Jr., and Sinke, G. C. 1969, *The Chemical Thermodynamics of Organic Compounds* (New York: Wiley).
Sultanov, R. G., Skripka, V. G., and Namiot, A. Yu. 1971, *Gazov. Promyshlennost*, **16**, 6.
———. 1972*a*, *Gazov. Promyshlennost*, **17**, 6.
———. 1972*b*, *Russian J. Phys. Chem.*, **46**, 1238.
Thorpe, T. E., and Tutton, A. E. 1890, *J. Chem. Soc.*, **57**, 545.
Tsiklis, D. S., Linshits, L. R., and Goryunova, N. P. 1965, *Russian J. Phys. Chem.*, **39**, 1590.
van Krevelen, D. W., Heftijzer, P. J., and Huntjens, F. J. 1949, *Rec. Trav. Chim.*, **68**, 191.
Wagman, D. D., Evans, W. H., Parker, V. B., Halow, I., Bailey, S. M., and Schumm, R. H. 1968, *Selected Values of Chemical Thermodynamic Properties: Tables for the First Thirty Four Elements in the Standard Order of Arrangement* (US NBS TN270-3).
Wallace, L. 1980, *Icarus*, **43**, 231.
Weidenschilling, S. J., and Lewis, J. S. 1973, *Icarus*, **20**, 465.

BRUCE FEGLEY, JR.: Building 54-1822, Department of Earth, Atmospheric, and Planetary Sciences, Massachusetts Institute of Technology, Cambridge, MA 02139

RONALD G. PRINN: Building 54-1824, Department of Earth, Atmospheric, and Planetary Sciences Massachusetts Institute of Technology, Cambridge, MA 02139